J. Non-Newtonian Fluid Mech. 165 (2010) 1139–1146

Contents lists available at ScienceDirect

Journal of Non-Newtonian Fluid Mechanics

journal homepage: www.elsevier.com/locate/jnnfm

Extensional dynamics of viscoplastic filaments: I. Long-wave approximation and the Rayleigh instability

N.J. Balmforth, Neville Dubash, Anja C. Slim *

Department of Mathematics, 1984 Mathematics Road, University of British Columbia, Vancouver, BC V6T 1Z2, Canada

ARTICLE INFO

Article history:
Received 10 August 2009
Received in revised form 8 May 2010
Accepted 29 May 2010

Keywords:
Viscoplastic fluids
Surface tension
Pinch-off

ABSTRACT

We derive an asymptotic reduced model for the extensional dynamics of long, slender, axisymmetric threads of incompressible Herschel–Bulkley fluids. The model describes the competition between viscoplasticity, gravity, surface tension and inertia, and is used to explore the viscoplastic Rayleigh instability. A finite-amplitude initial perturbation is required to yield the fluid and initiate capillary-induced thinning. The critical amplitude necessary for thinning depends on both the wavelength of the perturbation and on the yield stress. We also numerically examine the inertialess growth of the instability and the progression towards pinch-off. The final self-similar form of inertialess pinch-off is similar to that for a power-law fluid.

1. Introduction

The dynamics of how a liquid thread pinches into drops has excited the attention of fluid mechanicians for over three centuries. The systematic study of pinch-off in viscous fluids dates back at least as far as Savart, Plateau and Rayleigh in the 1800s, and nowadays the problem has developed into a common setting in which to study the competition between inertia, surface tension and fluid viscosity for Newtonian fluids. Comprehensive reviews of many aspects of extensional flows, for which thread breakup and drop formation problems are quintessential examples, are given by Eggers [1] and Eggers and Villermaux [2]. The viscoelastic version of the problem has also proved popular as it affords a means to explore and calibrate the effects of an elastic rheology (*e.g.* [3] and references therein). Indeed, a number of commercial devices exploit the detailed dynamics of viscoelastic filaments to perform rheometry.

By contrast, viscoplastic fluids have been studied very little in extension. Our goal in the current work is to provide a study of the extensional dynamics of viscoplastic filaments with a Herschel–Bulkley rheology. The study is split in two: in this first part we begin by deriving a theoretical model that captures the effects of surface tension, inertia and gravity in addition to the dominant rheological processes. All we demand is that the filament is axisymmetric and thin relative to its length, which allows us to take advantage of the slenderness of the configuration to simplify the governing fluid equations. We then apply the theory to study the so-called Rayleigh instability, the thinning and pinching of a uniform cylindrical jet of fluid driven by the action of surface tension, focusing for simplicity on the inertialess case. In the companion paper we consider two other problems: gravitationally induced dripping and thinning under imposed extension.

Slender filament models have been used extensively to provide a quantitatively accurate description compared to both simulations and experiments for Newtonian fluids (*e.g.* [4,5]) and to a lesser extent generalized Newtonian fluids (*e.g.* [6,7]). The predictions of the slender filament model can remain accurate even when the thread under consideration is not necessarily long and thin [4], but can fail under more extreme physical conditions [6,8,9].

The Rayleigh instability provides the simplest theoretical setting in which to study the dynamics underlying pinch-off in Newtonian fluids [1]. We consider the viscoplastic version for similar reasons, and explore whether the configuration also provides a similarly exemplary model. Unfortunately, it turns out that the viscoplastic Rayleigh instability is less natural than the corresponding Newtonian problem, largely because an undisturbed uniform filament is rigidly held by its yield stress, and the fluid structure cannot be broken by an infinitesimal perturbation. Instead, a finite initial stress perturbation is required and the subsequent dynamics depends on the detailed structure, rendering the problem more artificial. Nevertheless, our objectives in this paper are to gauge how yield stresses affect both capillary-induced extensional dynamics and the progression towards pinch-off, both of which can be conveniently studied within the relatively simple theoretical framework of the Rayleigh problem. We thereby set the stage for part II, in which we explore more realistic extensional flows.

* Corresponding author.
E-mail address: aslim@fas.harvard.edu (A.C. Slim).

0377-0257/$ – see front matter © 2010 Elsevier B.V. All rights reserved.
doi:10.1016/j.jnnfm.2010.05.012

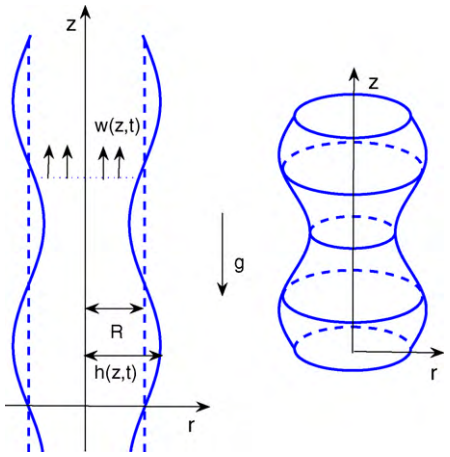

Fig. 1. The geometry of a long, slender filament.

Because we focus on the effect of the yield stress, the current article is distanced from earlier work focusing on generalized Newtonian fluids. Nonetheless, as surface tension drives the thinning of a thread, stresses grow substantially, suggesting that yield stresses play only a minor role in the limiting pinch-off dynamics. Indeed, we demonstrate explicitly that this is the case for inertialess, viscoplastic filaments. We therefore do not dwell on the details of pinch-off, but focus on the earlier dynamics which are more strongly influenced by the yield stress.

2. Theoretical model

2.1. Governing equations

The geometry of our problem is illustrated in Fig. 1: an axisymmetric thread of incompressible fluid described by the cylindrical polar coordinates, $(\hat{r}, \theta, \hat{z})$ with $\hat{z}$ directed vertically upwards, deforms within a dynamically passive exterior fluid. The filament's density is ρ and its rheology is modelled using the Herschel–Bulkley constitutive relation (*e.g.* [10]), with yield stress, τ_y, consistency, K, and power-law exponent, n.

The governing equations describing conservation of mass and momentum take the form

$$\frac{1}{\hat{r}}\frac{\partial}{\partial \hat{r}}(\hat{r}\hat{u}) + \frac{\partial \hat{w}}{\partial \hat{z}} = 0, \tag{1}$$

$$\rho\left(\frac{\partial \hat{u}}{\partial \hat{t}} + \hat{u}\frac{\partial \hat{u}}{\partial \hat{r}} + \hat{w}\frac{\partial \hat{u}}{\partial \hat{z}}\right) = -\frac{\partial \hat{p}}{\partial \hat{r}} + \frac{\partial \hat{\tau}_{rr}}{\partial \hat{r}} + \frac{\partial \hat{\tau}_{rz}}{\partial \hat{z}} + \frac{\hat{\tau}_{rr} - \hat{\tau}_{\theta\theta}}{\hat{r}}, \tag{2}$$

$$\rho\left(\frac{\partial \hat{w}}{\partial \hat{t}} + \hat{u}\frac{\partial \hat{w}}{\partial \hat{r}} + \hat{w}\frac{\partial \hat{w}}{\partial \hat{z}}\right) = -\frac{\partial \hat{p}}{\partial \hat{z}} + \frac{\partial \hat{\tau}_{rz}}{\partial \hat{r}} + \frac{\partial \hat{\tau}_{zz}}{\partial \hat{z}} + \frac{\hat{\tau}_{rz}}{\hat{r}} - \rho g, \tag{3}$$

where $\hat{t}$ is time, $(\hat{u}, 0, \hat{w})$ is the velocity field, $\hat{p}$ is pressure, and g is gravity. The constitutive relation for the deviatoric stress tensor $\hat{\boldsymbol{\tau}}$ is

$$\begin{cases} \hat{\boldsymbol{\tau}} = \begin{pmatrix} \hat{\tau}_{rr} & 0 & \hat{\tau}_{rz} \\ 0 & \hat{\tau}_{\theta\theta} & 0 \\ \hat{\tau}_{rz} & 0 & \hat{\tau}_{zz} \end{pmatrix} = (\tau_Y + K\hat{\dot{\gamma}}^n)\dfrac{\hat{\dot{\boldsymbol{\gamma}}}}{\hat{\dot{\gamma}}} & \text{if } \hat{\tau} > \tau_Y, \\ \hat{\dot{\boldsymbol{\gamma}}} = 0 & \text{otherwise,} \end{cases} \tag{4}$$

where the shear-rate tensor is given by

$$\hat{\dot{\boldsymbol{\gamma}}} = \begin{pmatrix} 2\dfrac{\partial \hat{u}}{\partial \hat{r}} & 0 & \dfrac{\partial \hat{w}}{\partial \hat{r}} + \dfrac{\partial \hat{u}}{\partial \hat{z}} \\ 0 & 2\dfrac{\hat{u}}{\hat{r}} & 0 \\ \dfrac{\partial \hat{w}}{\partial \hat{r}} + \dfrac{\partial \hat{u}}{\partial \hat{z}} & 0 & 2\dfrac{\partial \hat{w}}{\partial \hat{z}} \end{pmatrix}, \tag{5}$$

and $\hat{\dot{\gamma}} = \left[\hat{\dot{\boldsymbol{\gamma}}} : \hat{\dot{\boldsymbol{\gamma}}}/2\right]^{1/2}$ and $\hat{\tau} = [\hat{\boldsymbol{\tau}} : \hat{\boldsymbol{\tau}}/2]^{1/2}$ are the second invariants.

At the surface of the filament, $\hat{r} = \hat{h}(\hat{z}, \hat{t})$, we satisfy the kinematic condition,

$$\frac{\partial \hat{h}}{\partial \hat{t}} + \hat{w}\frac{\partial \hat{h}}{\partial \hat{z}} = \hat{u}, \tag{6}$$

together with the expression of force balance,

$$-\hat{p}\hat{\mathbf{n}} + \hat{\boldsymbol{\tau}}\cdot\hat{\mathbf{n}} = -\gamma\hat{\kappa}\hat{\mathbf{n}}, \tag{7}$$

where $\hat{\mathbf{n}} = (1, 0, -\partial\hat{h}/\partial\hat{z})/[1 + (\partial\hat{h}/\partial\hat{z})^2]^{1/2}$ is the outward normal to the thread, γ is the surface tension coefficient between the thread and the exterior fluid and the curvature $\hat{\kappa}$ is given by

$$\hat{\kappa} = \frac{1}{\hat{h}[1 + (\partial\hat{h}/\partial\hat{z})^2]^{1/2}} - \frac{\partial^2\hat{h}/\partial\hat{z}^2}{[1 + (\partial\hat{h}/\partial\hat{z})^2]^{3/2}}. \tag{8}$$

2.2. Scaling

The governing equations reduce to a simpler form when the thread is long and thin. The reduction is very similar to that for a Newtonian filament (*e.g.* [1,11]), and can be cast as a formal asymptotic expansion. Here, we mainly emphasize the generalizations required in the derivation for the Herschel–Bulkley constitutive relation.

For a slender filament, the geometrical limitation that the characteristic radius, R, is much less than a typical axial length-scale, L, implies a significant imbalance in the radial and axial derivatives. More specifically, if $\varepsilon = R/L \ll 1$ denotes the small aspect ratio of the filament, the imbalance in derivatives is expected to be $\partial/\partial\hat{z} \sim \varepsilon\partial/\partial\hat{r}$. Likewise, the geometry constrains the radial flow so that $\hat{u} \sim \varepsilon\hat{w}$. Thus, in (5) the components $(\hat{\dot{\gamma}}_{rr}, \hat{\dot{\gamma}}_{\theta\theta}, \hat{\dot{\gamma}}_{zz})$ all scale as U/R where U is a typical radial velocity.

The magnitude of the shear rate, $\hat{\dot{\gamma}}_{rz}$, requires more care: the simple estimate $\varepsilon^{-1}(U/R)$ is incorrect because the filament does not develop sufficient shear stress to drive significant internal shear, a well-known feature of free films and filaments (*e.g.* [1,11]). Instead, the axial velocity $\hat{w}$ is independent of radius to leading order and the relatively weak shear stresses generate a radially varying $O(\varepsilon^2)$ correction. Hence, $\partial\hat{w}/\partial\hat{r} \sim \partial\hat{u}/\partial\hat{z} \sim \varepsilon\partial\hat{w}/\partial\hat{z}$, and so $\hat{\dot{\gamma}}_{rz}$ scales as $\varepsilon U/R$. Moreover, since $w \approx w(z, t)$ the conservation of mass equation (1) also demands that

$$\frac{\partial \hat{u}}{\partial \hat{r}} = \frac{\hat{u}}{\hat{r}} = -\frac{1}{2}\frac{\partial \hat{w}}{\partial \hat{z}},$$

to leading order.

In view of the scaling of the deformation rates, it is apparent from the constitutive model that $\hat{\tau}_{rz}$ is $O(\varepsilon)$ smaller than the normal stress components, $(\hat{\tau}_{rr}, \hat{\tau}_{\theta\theta}, \hat{\tau}_{zz})$, in agreement with the notion that the filament does not develop substantial shear stress. The three terms involving the deviatoric stress on the right-hand side of (3) are therefore equally important; by contrast, the derivative of the shear stress is negligible on the right of (2). Moreover, $\hat{\tau}_{rr} = \hat{\tau}_{\theta\theta}$ to leading order, removing the final term of that equation. For the theoretical model, we further assume that the remaining terms in (2) also enter the dominant balance. Physically, this means that the (axial) extensional dynamics balances fluid stresses, gravity and inertia (with surface tension appearing later via the pressure boundary condition). Below, we see that this corresponds to adopting order one values for a number of dimensionless parameters.

In summary, to leading order

$$0 = -\frac{\partial \hat{p}}{\partial \hat{r}} + \frac{\partial \hat{\tau}_{rr}}{\partial \hat{r}}, \tag{9}$$

$$\rho\left(\frac{\partial\hat{w}}{\partial\hat{t}}+\hat{w}\frac{\partial\hat{w}}{\partial\hat{z}}\right)=-\frac{\partial\hat{p}}{\partial\hat{z}}+\frac{\partial\hat{\tau}_{rz}}{\partial\hat{r}}+\frac{\partial\hat{\tau}_{zz}}{\partial\hat{z}}+\frac{\hat{\tau}_{rz}}{\hat{r}}-\rho g. \tag{10}$$

A similar reduction of the full surface stress conditions from (7) furnishes (bearing in mind that $\partial\hat{h}/\partial\hat{z}=O(\varepsilon)$)

$$\hat{p}-\hat{\tau}_{rr}-\gamma\hat{\kappa}=\hat{\tau}_{rz}+\frac{\partial\hat{h}}{\partial\hat{z}}(\hat{p}-\hat{\tau}_{zz}-\gamma\hat{\kappa})=0 \tag{11}$$

on $\hat{z}=\hat{h}(\hat{z},\hat{t})$.

Thus far, all the scalings mimic the Newtonian problem. The main differences arise from further consideration of the constitutive relation, and in particular because the fluid need not be sufficiently stressed to yield. Indeed the preceding considerations implicitly assume that the fluid is yielded, since they are based on how the deformation rates then scale in order to maintain the slender geometry of the filament. For the yielded state, it then followed that $\hat{\tau}_{zz}=-2\hat{\tau}_{rr}=-2\hat{\tau}_{\theta\theta}$, which in turn implies that the yield condition is $\hat{\tau}=\sqrt{3}|\hat{\tau}_{zz}|/2>\tau_Y$ at leading order.

If $\hat{\tau}<\tau_Y$, the fluid is not yielded and $\hat{u}=\partial\hat{w}/\partial\hat{z}=0$. We cannot now use the constitutive relation to argue that the shear stress is much smaller than the normal stresses, upsetting our balancing of terms in the momentum equations, and the relation, $\hat{\tau}_{rr}=\hat{\tau}_{\theta\theta}$, no longer follows. Indeed, this difficulty is a necessary consequence of the fact that the stress state is formally indeterminate in the rigid state for viscoplastic models that do not incorporate any (viscoelastic) deformation below the yield stress, the force balance equations being insufficient to determine all the stress components uniquely.

To surmount this difficulty, we offer three arguments. First, one may appeal to regularizations of the constitutive model that prescribe the stress state even below yield: for a very viscous fluid or a linear viscoelastic solid, slight incompressible deformations still demand that the shear stress is much less than the normal stresses and $\hat{\tau}_{rr}=\hat{\tau}_{\theta\theta}$ with the geometry of our slender filament (for the same reasons as given above). Second, if the filament relaxed to a state at or below yield by deforming, then the temporal continuity of each stress component would preserve their relative scalings and enforce $\hat{\tau}_{rr}=\hat{\tau}_{\theta\theta}$. Third, if there were a significantly different pre-stress locked into unyielded fluid, the dynamics would partly reflect the release of that stress, leading to non-generic behaviour dependent on the specific stress state. In the interest of simplicity and because the choice seems most natural, we therefore adopt the same scalings and $\hat{\tau}_{rr}=\hat{\tau}_{\theta\theta}$ even when the fluid is below the yield stress.

2.3. One-dimensional approximation

We now integrate the governing mass and momentum equations (1), (9) and (10) across a cross-sectional slice, exploiting the reduced boundary conditions (6) and (11), to obtain the model system

$$\frac{\partial\hat{h}}{\partial\hat{t}}+\hat{w}\frac{\partial\hat{h}}{\partial\hat{z}}=-\frac{1}{2}\hat{h}\frac{\partial\hat{w}}{\partial\hat{z}}, \tag{12}$$

$$\rho\left(\frac{\partial\hat{w}}{\partial\hat{t}}+\hat{w}\frac{\partial\hat{w}}{\partial\hat{z}}\right)=-\gamma\frac{\partial\hat{\kappa}}{\partial\hat{z}}+\frac{3}{2\hat{h}^2}\frac{\partial}{\partial\hat{z}}(\hat{h}^2\hat{\tau}_{zz})-\rho g, \tag{13}$$

and

$$\hat{\tau}_{zz}=2\left(\frac{\tau_Y}{\hat{\dot{\gamma}}}+K\hat{\dot{\gamma}}^{n-1}\right)\frac{\partial\hat{w}}{\partial\hat{z}}\quad\text{if }\hat{\tau}>\tau_Y, \tag{14}$$

$$\frac{\partial\hat{w}}{\partial\hat{z}}=0\quad\text{otherwise}, \tag{15}$$

where $\hat{\dot{\gamma}}=\sqrt{3}\left|\partial\hat{w}/\partial\hat{z}\right|$.

Note that in (13), we retain the full surface curvature given by (8). In a formal asymptotic theory, one would keep only the leading-order contribution, $\hat{\kappa}\approx 1/\hat{h}$. However, in many previous studies of the Newtonian problem the full form of the curvature has been retained to incorporate additional effects of surface tension in a non-asymptotic fashion. We follow suit here, and do not approximate the curvature formula (8), except for analytical convenience where explicitly stated.

2.4. Non-dimensionalization

We remove dimensions from (12) to (15) using the initial radius of the thread, R, and the viscous-capillary time-scale, $T=(KR/\gamma)^{1/n}$, as characteristic scales. We then set

$$\hat{t}=Tt,\qquad(\hat{z},\hat{h})=R(z,h),\qquad\hat{w}=RT^{-1}w,$$
$$(\hat{p},\hat{\tau}_{zz})=KT^{-n}(p,\tau_{zz}),\qquad\hat{\dot{\gamma}}=T^{-1}\dot{\gamma},\qquad\hat{\kappa}=R^{-1}\kappa,$$

which furnishes the dimensionless equations,

$$\frac{\partial h}{\partial t}+w\frac{\partial h}{\partial z}=-\frac{1}{2}h\frac{\partial w}{\partial z}, \tag{16}$$

$$\mathcal{R}\left(\frac{\partial w}{\partial t}+w\frac{\partial w}{\partial z}\right)=-\frac{\partial\kappa}{\partial z}+\frac{3}{2h^2}\frac{\partial}{\partial z}(h^2\tau_{zz})-G, \tag{17}$$

with

$$\kappa=\frac{1}{h[1+(\partial h/\partial z)^2]^{1/2}}-\frac{\partial^2h/\partial z^2}{[1+(\partial h/\partial z)^2]^{3/2}}. \tag{18}$$

We also rewrite the constitutive relation in the alternative form,

$$\frac{\partial w}{\partial z}=\frac{1}{\sqrt{3}}sgn(\tau_{zz})\left[\max\left(\frac{\sqrt{3}}{2}|\tau_{zz}|-\beta,0\right)\right]^{1/n}, \tag{19}$$

incorporating both the yielded and rigid phases.

A number of dimensionless parameters appear (besides the power-law exponent n):

$$R=\frac{\rho R^3}{\gamma}\left(\frac{\gamma}{KR}\right)^{2/n},\qquad G=\frac{\rho gR^2}{\gamma},\qquad\beta=\frac{\tau_YR}{\gamma}.$$

These parameters are the square of the inverse Ohnesorge number, which measures the importance of inertia relative to viscosity (and can be interpreted as the square of the ratio of the inertial time-scale to the viscous time-scale), the gravitational Bond number, and a number measuring the importance of the yield stress relative to surface tension.

3. Rayleigh instability

For Newtonian fluids, linear stability analysis of a uniform cylindrical thread in the absence of gravity predicts that infinitesimal perturbations of the profile are unstable if their wavelengths exceed 2π (the so-called Rayleigh instability): such perturbations increase (decrease) the surface tension stress in the slightly thinner (thicker) regions, driving further narrowing (widening) of the thread. For a viscoplastic fluid, on the other hand, the situation is different: our initial, uniform thread is held rigid by the fluid's yield stress and the additional surface tension stress generated by an infinitesimal perturbation is never sufficient to overcome a finite yield stress. Instead, a perturbation of finite amplitude is required to allow surface tension to stress the column sufficiently to liquefy it somewhere along its length; and conventional linear stability theory is no longer relevant (as in some other viscoplastic stability problems; *e.g.* [12]). Specifically, we consider a spatially periodic problem and introduce a finite-amplitude perturbation by initially deforming the thread

profile:

$$h(z,0) = 1 + h_1 \cos\left(\frac{2\pi z}{\lambda}\right), \tag{20}$$

where λ is the wavelength (or domain length).

3.1. Inertialess instability

To simplify our analysis, we neglect inertia, $\mathcal{R} = 0$, and approximate the curvature as

$$\kappa = \frac{1}{h} - \frac{\partial^2 h}{\partial z^2},$$

to allow certain results to be obtained in closed form. Then, integrating the right-hand side of (17), we obtain

$$\tau_{zz} = \frac{f(t)}{h^2} - \frac{2}{3h^2}\int_0^z \left(\frac{\partial h}{\partial z} + h^2\frac{\partial^3 h}{\partial z^3}\right) dz, \tag{21}$$

where the "constant" of integration, $f(t)$, is proportional to the extensional force on the thread at $z=0$. If the initial stress predicted by (21) is everywhere below the yield value, $2\beta/\sqrt{3}$, the thread remains rigid, $w(z,t) = 0$, and $f(t)=f(0)$ is undetermined. The unknown stress, $f(0)/h(z,0)^2$, reflects the indeterminacy of the stress state of the rigid, uniform filament (which is constrained, but not eliminated, by the expedient asymptotic scalings that we adopted in deriving the slender filament model). The magnitude of this pre-stress is limited by the requirement that the thread does not yield, but is otherwise arbitrary.

Conversely, if (21) predicts that yielding occurs somewhere, then $f(t)$ is determined by imposing the periodicity condition,

$$0 = w(\lambda,t) - w(0,t) = \int_0^\lambda \frac{\partial w}{\partial z} dz, \tag{22}$$

with the integrand given by (19) and (21) (*cf.* [13]).

3.1.1. Criteria for instability and yielding

To conserve mass when liquefied, the thread must yield in at least two separate regions; one in a state of extension, $\tau_{zz} > 2\beta/\sqrt{3}$ (and hence $\partial w/\partial z > 0$), the other under compression, $\tau_{zz} < -2\beta/\sqrt{3}$ ($\partial w/\partial z < 0$). Thus, the criterion for the thread to first liquefy is $\max\{\tau_{zz}\} = -\min\{\tau_{zz}\} = 2\beta/\sqrt{3}$. For our initial condition (20), this occurs when h_1 is increased beyond some threshold depending on the yield-stress parameter, β.

The threshold follows from substituting the initial condition (20) into (21) to obtain the initial stress

$$\tau_{zz}(z,0) = \frac{f(0)}{h^2} - \frac{2}{3h^2}\left(h - h_0 - \frac{4\pi^2}{3\lambda^2}(h^3 - h_0^3)\right),$$

where $h_0 = h(0,0) = 1 + h_1$. For sufficiently small amplitudes, the only stress extrema occur at $z=0$ and $\lambda/2$. Thus, the fluid can only yield if

$$\beta > \frac{1}{\sqrt{3}}\frac{h_1}{1+h_1^2}\left|\frac{4\pi^2}{3\lambda^2}(3+h_1^2) - 1\right|. \tag{23}$$

For longer waves with $\lambda > 2\pi$, we further find $\tau_{zz}(0,0) = -2\beta/\sqrt{3}$ and $\tau_{zz}(\lambda/2,0) = 2\beta/\sqrt{3}$. Because $w = 0$ at the extremal points, (16) becomes $\partial h/\partial t = -(h/2)\partial w/\partial z$ there, and so $h(0,t)$ increases and $h(\lambda/2,t)$ decreases from the initial condition. The thread therefore proceeds unstably towards pinch-off. Conversely for shorter waves with $\lambda < 2\pi$, the extrema of the stress are reversed, $\tau_{zz}(0,0) = 2\beta/\sqrt{3}$ and $\tau_{zz}(\lambda/2,0) = -2\beta/\sqrt{3}$, as are the senses of $\partial h/\partial t$ at $z=0$ and $\lambda/2$. Hence the shape deformations become stably smoothed by surface tension.

For larger amplitudes, because of the increasing contribution of the axial curvature term (which has a locally stabilising effect) to the surface tension force, the global stress extrema need not lie at $z=0$ or $\lambda/2$. When this occurs the location of the stress extrema, together with the amplitude thresholds, must be computed numerically. For example, Fig. 2 shows critical amplitudes as a function of β for various values of the wavelength. Numerically computed thresholds are given by the solid lines; the dashed lines show the prediction in (23). The two sets of curves diverge at larger values of h_1, where the stress extrema shift from the profile extrema. Sample stress profiles illustrating how the stress extrema first shift away from $z=0$, $\lambda/2$ are shown in Fig. 3.

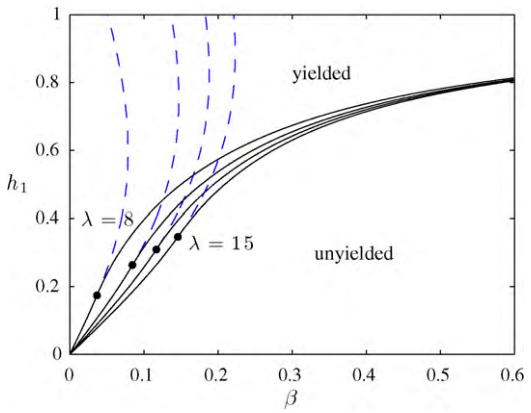

Fig. 2. Threshold amplitudes (solid curves) for yielding at unstable wavelengths with $\lambda = 8, 10, 12, 15$. The dashed lines are given by the small-amplitude calculation, (23), and the larger dots denote where (23) deviates from the true solution (i.e., where the global stress extrema cease to occur at $z=0$ and $\lambda/2$).

3.1.2. Thread evolution

To study the thinning dynamics in more detail, we solve (16), (19), (21) and (22) numerically by first discretizing in space (using a uniform grid with 2000 points), and then integrating the resulting coupled ordinary differential equations with a standard integrator with an adaptive time step. The one complication is the determination of $f(t)$ from the nonlinear constraint, (19) and (21), which requires an iterative procedure. Computations begin with a stationary perturbed cylinder and are carried out until the minimum radius reached $h_{\min} < 10^{-3}$.

An example showing the evolution from an unstably perturbed thread is shown in Fig. 4 ($\beta = 0.03$, $\lambda = 10$, $h_1 = 0.1$, and $n = 1$; with these values for β and λ, the threshold amplitude is $h_1 = 0.087$). The first panel in the figure displays the thread profile at various times;

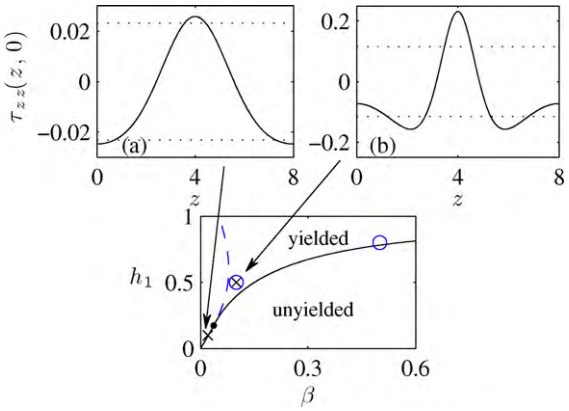

Fig. 3. The initial stress distribution, $\tau_{zz}(z,0)$, for (a) $h_1 = 0.1$, $\beta = 0.02$ and (b) $h_1 = 0.5$, $\beta = 0.1$ ($\lambda = 8$). The dotted lines represent the yield stress. The lower panel is a reproduction of the threshold amplitude curve for $\lambda = 8$ from Fig. 2 with the crosses showing the relative locations of the stress profiles in the parameter space. The circles show the parameter values of the threads shown in Fig. 5.

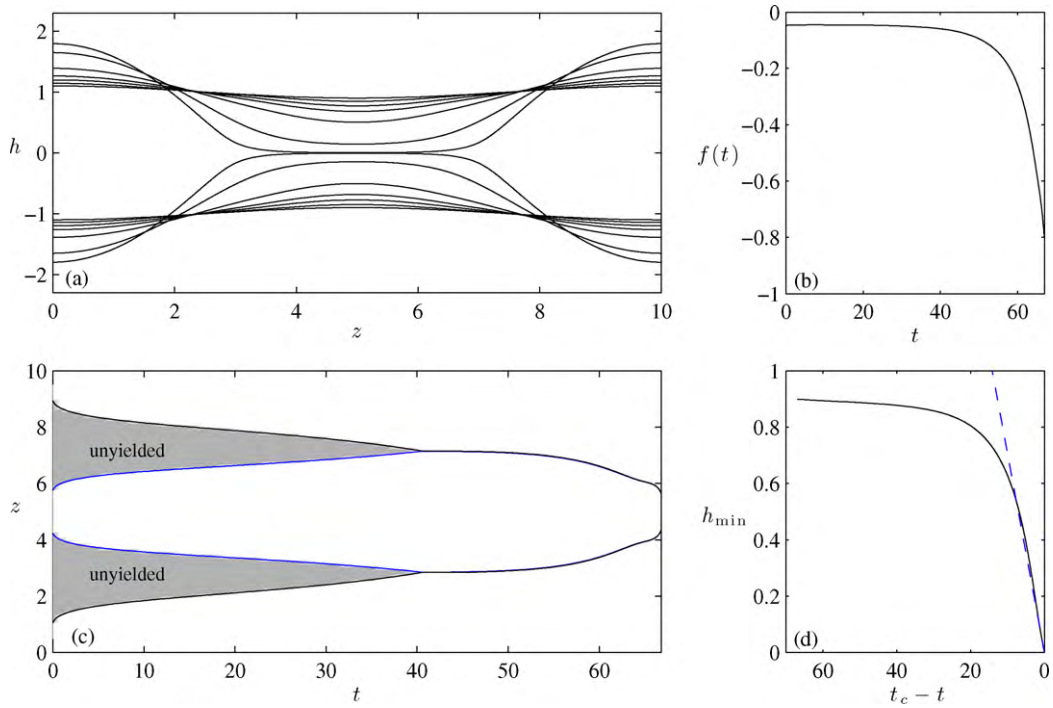

Fig. 4. The evolution of an unstable thread: $\beta = 0.03$, $\lambda = 10$, $h_1 = 0.1$, $n = 1$. (a) The thread profile $h(z,t)$ at times $t = 0$, 40, 50, 55, 60, 65, 66 (pinch-off occurs for $t_c \approx 66.89$). (b) A time series of $f(t)$. (c) The location of the yield surfaces as a function of time. Shaded regions are unyielded. Though the two surfaces appear to merge around time $t = 40$, there is still a very narrow unyielded region for $t > 40$. (d) The minimum radius, $h_{\min}(t) \equiv h(\lambda/2, t)$, as a function of time. The dashed line represents (24).

extrapolation suggests that pinch-off occurs at $t_c \approx 66.9$. The second, third and fourth panels show the time series of $f(t)$, the position of the yield surfaces and the minimum radius, $h_{\min}(t) \equiv h(\lambda/2, t)$, respectively. Initially, only small portions of the thread near $z = 0$ ($z = \lambda$) and $z = \lambda/2$ are yielded ((23) applies in this example; *cf.* Fig. 3a). However, the yielded regions quickly expand to fill the thread. Note that small unyielded regions always surround the positions at which the stress (or $\partial w/\partial z$) changes sign. However, as the thread evolves, the stress increases by several orders of magnitude over the remainder of the thread and the unyielded region becomes extremely narrow, with the two yield surfaces appearing to merge together in Fig. 4b. Although the unyielded (plug) regions

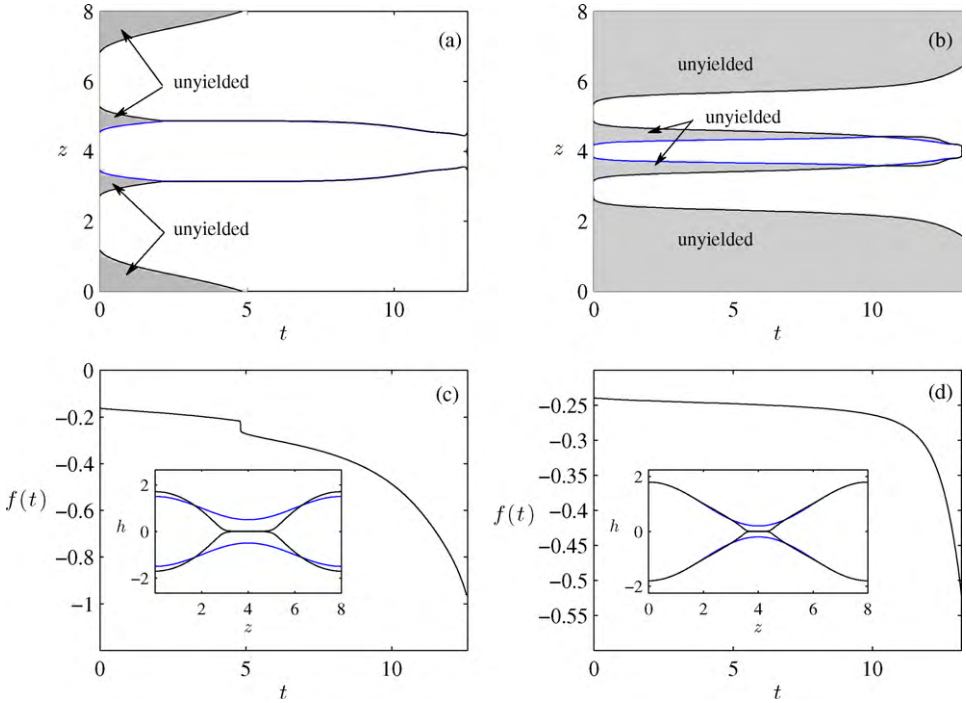

Fig. 5. (a) The location of the yield surfaces as a function of time for $\beta = 0.1$, $\lambda = 8$, $h_1 = 0.5$, $n = 1$. Shaded regions are unyielded. (The threshold amplitude for yielding is $h_1 = 0.396$, and pinch-off occurs at $t_c \approx 12.6$.). (b) The location of the yield surfaces as a function of time for $\beta = 0.5$, $\lambda = 8$, $h_1 = 0.8$, $n = 1$. (The threshold amplitude for yielding is $h_1 = 0.781$, and pinch-off occurs at $t_c \approx 13.2$.) (c) and (d) Time series of $f(t)$ corresponding to (a) and (b) respectively, with the insets showing the initial thread profile and the profile just before pinch-off.

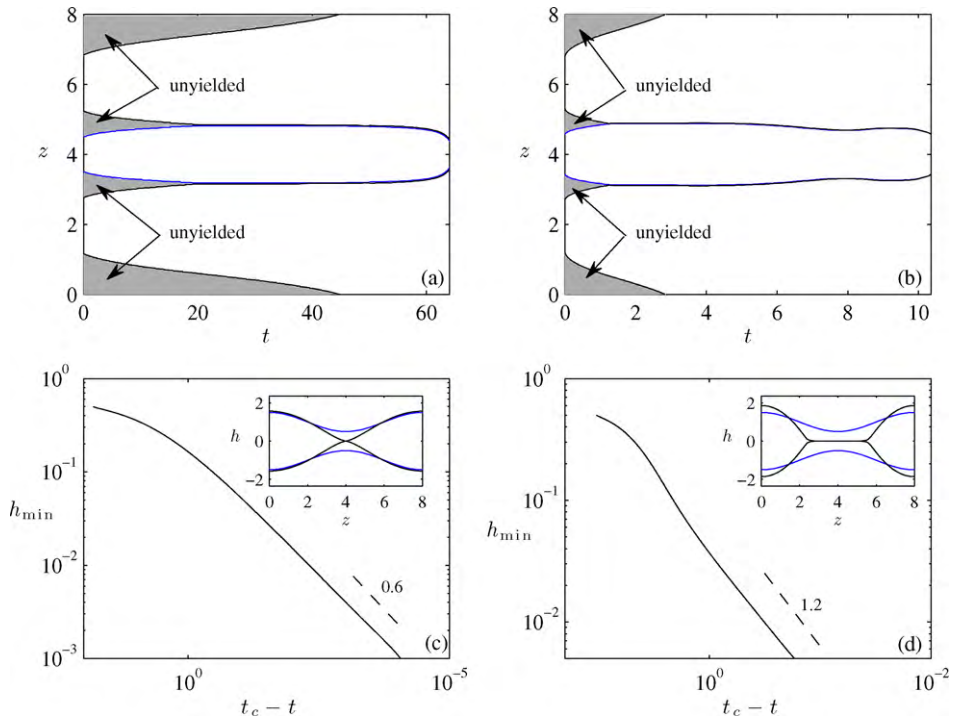

Fig. 6. (a) The location of the yield surfaces as a function of time for $\beta = 0.1$, $\lambda = 8$, $h_1 = 0.5$, $n = 0.6$. Shaded regions are unyielded. (b) The location of the yield surfaces as a function of time for $\beta = 0.1$, $\lambda = 8$, $h_1 = 0.5$, $n = 1.2$. (c) and (d) The minimum radii, $h_{\min}(t) \equiv h(\lambda/2, t)$, as functions of time, corresponding to (a) and (b) respectively. The expected slope near pinch-off, $(t_c - t)^n$, is indicated by the dashed lines. The insets show the initial thread profile and the profile just before pinch-off.

are hard to resolve at times close to pinch-off, there is no evidence that they play a dynamical role.

Further examples, for larger values of β, are shown in Fig. 5. In these cases, the stress extrema do not both lie at the stagnation points (the minimum stresses occur near $z \approx 2.5$, *cf.* Fig. 3b), and the region around $z = 0$ is initially rigid. For the case shown in Fig. 5a and c the plug around $z = 0$ quickly liquefies to leave a pinching state much like that shown earlier, as highlighted by the thread profiles inset into Fig. 5c. However, at large values of β this plug remains intact for the entire evolution of the thread (Fig. 5b and d). At even higher values of β the behaviour is qualitatively similar to that shown in Fig. 5b and d, though by this point the threshold amplitudes necessary to yield the fluid thread are very large (*e.g.*, for $\beta \approx 1$ the critical amplitudes are around $h_1 \approx 0.9$).

Finally, the evolution for threads with different power-law indices are shown in Fig. 6. Qualitatively the overall behaviour is similar to the case of $n = 1$; however, there is a distinct difference in the thread profiles for differing values of the power-law index. For $n < 1$ the central neck region near $h_{\min}(t) \equiv h(\lambda/2, t)$ is shorter, and the plug regions persist for longer periods of time. These are a result of the decreasing resistance to stress due to the shear thinning nature of the fluid. For $n > 1$ we have the opposite behaviour: the central neck region becomes longer and the plug regions liquefy more quickly.

3.1.3. Approach to pinch-off

As illustrated by the narrowing of the plugs in Figs. 4 and 5, the extensional stresses dominate the yield stress over the thinning regions as the thread progresses towards pinch-off. Indeed, as illustrated by the minimum radius, $h_{\min}(t)$, displayed in Fig. 4d, the solution appears to converge to the self-similar form expected for a Newtonian filament, with [1,14]

$$h_{\min}(t) \approx 0.0709(t_c - t), \tag{24}$$

where t_c is the time of pinch-off. (The same curve, shown on a logarithmic scale, is given later in Fig. 8c). Similarly for $n \neq 1$ the solutions appear to converge to the inertialess self-similar form for power-law fluids (the large extension limit for all generalized Newtonian models), with the minimum radius then scaling like $(t_c - t)^n$; see Fig. 6c and d [15–17].

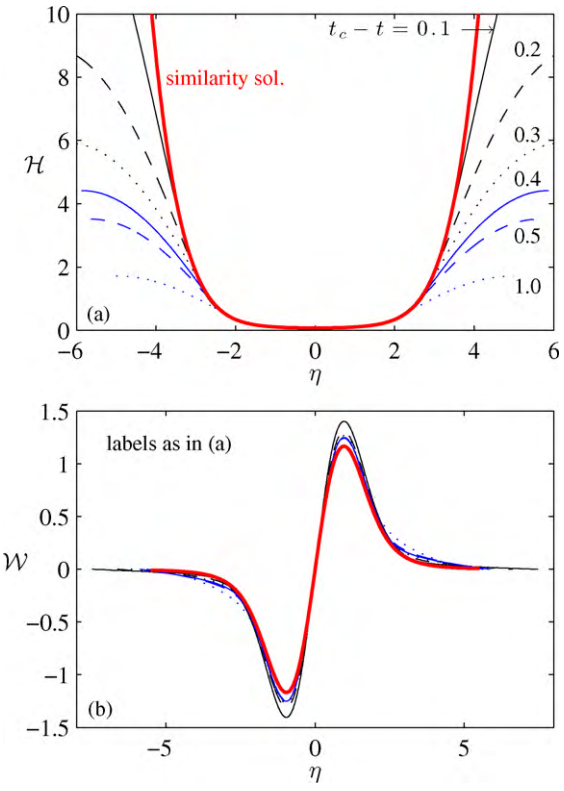

Fig. 7. Collapse towards the self-similar solution for (a) the thread profiles and (b) the velocity. ($\beta = 0.03$, $\lambda = 10$, $h_1 = 0.1$, $n = 1$, $a \approx 0.175$).

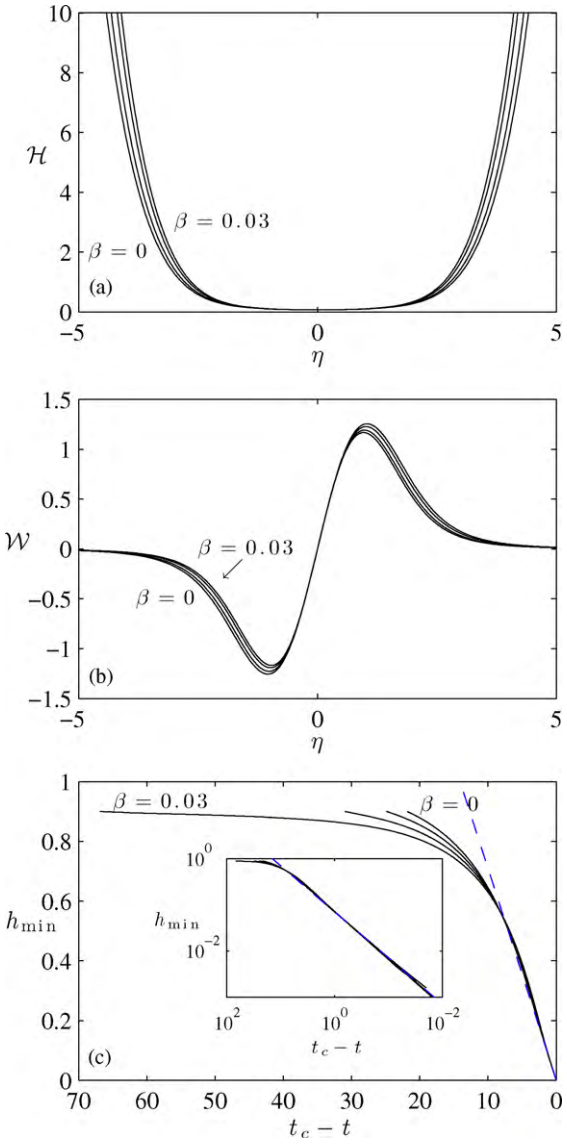

Fig. 8. The different similarity solutions obtained for $\beta = 0, 0.01, 0.02, 0.03$, ($\lambda = 10$, $h_1 = 0.1$, $n = 1$, $a \approx 0.175$). (a) The thread profile; (b) the velocity; (c) the minimum radius as a function of time for $\beta = 0, 0.01, 0.02, 0.03$; the dashed line represents (24), the inset shows the same data on a logarithmic scale.

Further details of the self-similar solutions (for $n = 1$) are shown in Figs. 7 and 8. Fig. 7 shows the collapse of numerical solutions under the Newtonian similarity scalings,

$$\eta = (t_c - t)^{-a}(z - \frac{1}{2}\lambda), \qquad H(\eta) = \frac{h(z,t)}{t_c - t}, \tag{25}$$

$$\mathcal{W}(\eta) = (t_c - t)^{1-a} w(z,t), \qquad \mathcal{T}(\eta) = (t_c - t)\tau_{zz}(z,t) \tag{26}$$

(see [14]), where a is a suitable eigenvalue arising because the similarity solution is of the second kind. Note that, although Figs. 4d and 7 suggest that our numerical solutions converge to the Newtonian similarity solution (where $a \approx 0.175$), the yield stress is not irrelevant. In fact, because the similarity solution is of the second kind, the detailed form contains a constant (in addition to the eigenvalue a), which must be matched to the filament profile and velocity outside the pinching region. In the Newtonian case, the value of this constant (the effect of which is to scale the similarity solution $\mathcal{H}(\eta)$ in η), depends on the initial perturbation amplitude [14]. With a yield stress both the spatial structure of the similarity solution and the additional constant depend on β, as illustrated in Fig. 8. The scaling constant in the similarity solutions is calculated by matching the scaled thread profile, $\mathcal{H}(\eta)$, at $t_c - t = 0.01$ to the analytic similarity solution at a fixed value of $\mathcal{H}$ (here we used $\mathcal{H} = 2$, though the result is unaffected by the specific value).

The scalings in (25) and (26) also confirm our numerical observation that the shrinking plugs in Figs. 4 and 5 do not affect the pinching dynamics: the yield stress is order $(t_c - t)$ less than the local stress everywhere except in narrow regions surrounding the stress-free points, $\eta = \eta_*$, where $\mathcal{T}(\eta_*) = 0$. Indeed, since $\mathcal{T}(\eta) = \pm 2\beta(t_c - t)/\sqrt{3}$ at the edges of the plugs, those rigid sections have the borders,

$$\eta \sim \eta_* \pm \frac{2\beta(t_c - t)}{\mathcal{T}'(\eta_*)\sqrt{3}}, \tag{27}$$

or

$$z \sim \lambda/2 + \eta_*(t_c - t)^a \pm \frac{2\beta(t_c - t)^{a+1}}{\mathcal{T}'(\eta_*)\sqrt{3}}. \tag{28}$$

In other words, the plugs move towards the pinch points, $z = \lambda/2$ at the rate $(t_c - t)^a$, but their width shrinks faster still, like $(t_c - t)^{a+1}$. Moreover, the similarity scalings, together with the integral of the momentum equation in (21), can be used to show that there is no significant change in the thread profile across the plugs. Thus, although the plugs enter the self-similar regions as the thread progresses towards pinch-off, their effect disappears.

For Newtonian filaments, inertia cannot remain negligible as the thread pinches off and must eventually enter the main balance of forces together with surface tension and viscous forces. This leads to another self-similar solution in which the minimum radius again decreases linearly with time, but the pre-factor on the right-hand side of (24) is adjusted to 0.0304 (*e.g.* [18,19]). This solution is of the first kind and independent of the dynamics outside the pinching region. Although we have not taken steps to confirm this, we anticipate that the yield stress does not change this picture, and so the self-similar scaling seen in Fig. 4d is only a transient precursor to the final behaviour [20,21,22].

4. Conclusions

In this article we have developed a slender filament model for Herschel–Bulkley fluids that incorporates the effects of surface tension, inertia, gravity and rheology. We have applied this model to explore the viscoplastic analogue of the Rayleigh instability and, in part II, will use it to study viscoplastic dripping and bridges.

For the Rayleigh problem, a filament with a yield stress is linearly stable and finite-amplitude perturbations are required to kick the column into action. We calculated the conditions for yielding and instability of a sinusoidally perturbed thread based on the initial amplitude and wavelength. We also numerically studied the inertialess growth of the instability and the progression towards pinch-off. Because the pinching dynamics now depends on the detailed fashion in which the column is initially liquefied, the Rayleigh instability for a viscoplastic fluid becomes rather artificial and cannot be considered to be the fundamental problem that it is for Newtonian (and power-law) fluids. Instead, it is more natural to consider situations in which the thread is forced to yield by external forces or properly controlled perturbations, as in the drip and bridge problems of part II; these scenarios are relatively simple to set up as laboratory experiments, and have many direct applications.

The Rayleigh problem does highlight the key result that the yield stress does not play a major role in the self-similar dynamics near pinch-off: we have argued that sufficiently close to the moment that the thread breaks, the behaviour is similar to that expected for Newtonian and power-law fluids, reflecting the dominance of the viscous forces over yield stress. Thus, the final pinch-off

reflects only the balance of surface tension, viscosity and inertia (at least for power-law indices that are neither too small nor too large [8,17]).

References

[1] J. Eggers, Nonlinear dynamics and breakup of free-surface flows, Rev. Modern Phys. 69 (1997) 865–929.
[2] J. Eggers, E. Villermaux, Physics of liquid jets, Rep. Prog. Phys. 71 (2008) 036601.
[3] G.H. McKinley, T. Sridhar, Filament-stretching rheometry of complex fluids, Annu. Rev. Fluid Mech. 34 (2002) 375–415.
[4] J. Eggers, T.F. Dupont, Drop formation in a one-dimensional approximation of the Navier–Stokes equation, J. Fluid Mech. 262 (1994) 205–221.
[5] B. Ambravaneswaran, E.D. Wilkes, O.A. Basaran, Drop formation from a capillary tube: comparison of one-dimensional and two-dimensional analyses and occurrence of satellite drops, Phys. Fluids 14 (2002) 2606.
[6] O.E. Yildirim, O.A. Basaran, Deformation and breakup of stretching bridges of Newtonian and shear-thinning liquids: comparison of one-and two-dimensional models, Chem. Eng. Sci. 56 (1) (2001) 211–233.
[7] V. Dravid, P.B. Loke, C.M. Corvalan, P.E. Sojka, Drop formation in non-Newtonian jets at low Reynolds numbers, J. Fluids Eng. 130 (2008) 081504.
[8] P. Doshi, O.A. Basaran, Self-similar pinch-off of power law fluids, Phys. Fluids 16 (2004) 585.
[9] A.U. Chen, P.K. Notz, O.A. Basaran, Computational and experimental analysis of pinch-off and scaling, Phys. Rev. Lett. 88 (17) (2002) 174501.
[10] R.B. Bird, G.C. Dai, B.J. Yarusso, The rheology and flow of viscoplastic materials, Rev. Chem. Eng. 1 (1) (1983) 1–70.
[11] A. Oron, S.H. Davis, S.G. Bankoff, Long-scale evolution of thin liquid films, Rev. Modern Phys. 69 (1997) 931–980.
[12] N.J. Balmforth, A. Rust, Weakly nonlinear viscoplastic convection, J. Non-Newtonian Fluid Mech. 158 (2009) 36–45.
[13] G.H. McKinley, A. Tripathi, How to extract the Newtonian viscosity from capillary breakup measurements in a filament rheometer, J. Rheol. 44 (2000) 653.
[14] D.T. Papageorgiou, On the breakup of viscous liquid threads, Phys. Fluids 7 (1995) 1529–1544.
[15] M. Renardy, Self-similar jet breakup for a generalized PTT model, J. Non-Newton. Fluid Mech. 103 (2002) 261–269.
[16] P. Doshi, R. Suryo, O.E. Yildirim, G.H. McKinley, O.A. Basaran, Scaling in pinch-off of generalized Newtonian fluids, J. Non-Newton. Fluid Mech. 113 (1) (2003) 1–27.
[17] M. Renardy, Y. Renardy, Similarity solutions for breakup of jets of power law fluids, J. Non-Newton. Fluid Mech. 122 (1–3) (2004) 303–312.
[18] J. Eggers, Universal pinching of 3D axisymmetric free-surface flow, Phys. Rev. Lett. 71 (21) (1993) 3458–3460.
[19] M.P. Brenner, J.R. Lister, H.A. Stone, Pinching threads, singularities and the number 0.0304. . ., Phys. Fluids 8 (11) (1996) 2827–2836.
[20] J.R. Lister, H.A. Stone, Capillary breakup of a viscous thread surrounded by another viscous fluid, Phys. Fluids 10 (1998) 2758.
[21] A. Rothert, R. Richter, I. Rehberg, Transition from symmetric to asymmetric scaling function before drop pinch-off, Phys. Rev. Lett. 87 (8) (2001) 84501.
[22] J. Eggers, Drop formation-an overview, Z. Angew. Math. Mech. 85 (6) (2005) 400–410.